Journal of Power Sources 248 (2014) 180–189

Contents lists available at ScienceDirect

Journal of Power Sources

journal homepage: www.elsevier.com/locate/jpowsour

Effects of precursor, synthesis time and synthesis temperature on the physical and electrochemical properties of $Li(Ni_{1-x-y}Co_xMn_y)O_2$ cathode materials

Zhongling Xu [a, b], Lingli Xiao [b], Fei Wang [b], Kuichen Wu [b], Liutao Zhao [b], Man-Rong Li [b, c], Hong-Li Zhang [d], Qingguo Wu [b], Jianbo Wang [a, *]

[a] School of Physics and Technology, Center for Electron Microscopy and MOE Key Laboratory of Artificial Micro- and Nano-Structures, Wuhan University, Wuhan 430072, China
[b] Zhejiang WELLY Energy Corporation, 48 Xingyuan Rd, Cixi, Zhejiang 315301, China
[c] Department of Chem. & Chem. Bio., Rutgers, The State University of New Jersey, 610 Taylor Rd., Piscataway, NJ 08854, USA
[d] Ningbo Shijie New Energy Technology LLC, 108 Zhongxing East, Cixi, Zhejiang 315301, China

HIGHLIGHTS

- Small precursor primary particle means big primary particle and good cyclability of NCM.
- Long reaction time results in improved electrochemical properties of NCM.
- High synthesis temperature means big primary/secondary particles and low tap density of NCM.
- $Li(Ni_{1/3}Co_{1/3}Mn_{1/3})O_2$ synthesized at 950 °C has the best electrochemical performance.
- A higher synthesis temperature is needed when Ni content of NCM is low.

ARTICLE INFO

Article history:
Received 28 July 2013
Received in revised form
10 September 2013
Accepted 15 September 2013
Available online 24 September 2013

Keywords:
Lithium-ion batteries
Cathode materials
Layered oxide
Solid-state reaction

ABSTRACT

The effects of the synthesis temperature, the synthesis time and the nature of the transition-metal hydroxide precursors on the physical and electrochemical properties of $Li(Ni_{1-x-y}Co_xMn_y)O_2$ synthesized using solid-state reactions are studied. Higher synthesis temperature results in larger primary and secondary particle sizes, a lower tap density and a broader secondary particle size distribution. Increase in reaction time improves the crystallinity and the cyclability. A smaller primary particle size of the precursor leads to a larger primary particle size of $Li(Ni_{1-x-y}Co_xMn_y)O_2$. $Li(Ni_{1-x-y}Co_xMn_y)O_2$ with a better crystallinity, a well-defined layered structure and a better cation ordering exhibits a higher capacity, a better cycling performance and rate capability. The optimized synthesis conditions for precursors NCMOH111-α and NCMOH424-a is 950 °C for 12 h and 950 °C for 9 h, respectively. NCM111-α-950-12h delivers a discharge capacity of 165.5 mAh g^{-1} during the initial cycle at a rate of 0.1C with a columbic efficiency of 87%, a 3C rate capability of 91.25% and a 1C capacity retention rate of 98.25% after 40 cycles.

1. Introduction

Lithium-ion batteries (LIBs), which have much higher volume/weight energy and power densities than other secondary batteries, are eligible for applications in transportation (e.g., electric vehicles and plug-in hybrid electric vehicles) and renewable energy storage, such as solar, wind and tidal energy. Although LIBs have been extensively studied over the past decades, they still face big challenges in meeting the high requirements of new applications, for example, the cost and safety issues for large-scale batteries. Developing novel battery materials and optimizing the currently used materials are two main routes to improve the performance of LIBs and to further extend their applications. Recently, a layer-structured transition-metal oxide $Li(Ni_{1-x-y}Co_xMn_y)O_2$ (NCM), which is an analog of $LiCoO_2$, has been widely studied as a promising substitute for $LiCoO_2$ as the cathode material for high-performance LIBs due to its lower cost, better rate capability and cyclability, lower toxicity and higher specific capacity [1–6]. The

* Corresponding author. Tel.: +86 27 6875 2481x3106; fax: +86 27 6875 2569.
E-mail address: wang@whu.edu.cn (J. Wang).

0378-7753/$ – see front matter © 2013 Elsevier B.V. All rights reserved.
http://dx.doi.org/10.1016/j.jpowsour.2013.09.064

performance of this multi-elemental cathode material is highly sensitive to the synthesis conditions, which directly determine its composition and physical properties, including its primary particle size (PPS), morphology, crystal structure, crystallinity, structural perfection, and level of cation ordering. Currently, a hydroxide coprecipitation method combined with a solid-state sintering reaction is the most controllable method for large-scale industrial production of this NCM cathode [7–10]. Although some NCM compounds have been successfully commercialized, the effects of the synthesis parameters, such as the synthesis temperature, the reaction time and the properties of the precursor, on the physical properties and final electrochemical performance of NCM are not yet well understood, especially on the level of industrial production.

In our previous work [11], the effects of the precursors and synthesis conditions on the physical and electrochemical properties of the layered $Li(Ni_{0.5}Co_{0.2}Mn_{0.3})O_2$ (NCM523) compound were investigated. Here, we extend our research to the optimization of the synthesis of other NCM oxides, $Li(Ni_{1/3}Co_{1/3}Mn_{1/3})O_2$ (NCM111) and $Li(Ni_{0.4}Co_{0.2}Mn_{0.4})O_2$ (NCM424), report the optimized synthesis conditions for each oxide (NCM111 and NCM424) and compare them with previous results for NCM523. The NCM111 cathode obtained under optimized conditions delivers an initial discharge capacity of 165.5 mAh g^{-1} at 0.1C and a capacity retention rate of 98.25% at 1C after 40 cycles. The present results will provide useful information for the systematic optimization of the synthesis of the NCM cathode family.

2. Experiments

Five commercially supplied NCM hydroxides precursors (NCMOH)—NCMOH111-α (Fengyuan Power, China), NCMOH111-β (Oriental Tanye, China), NCMOH111-γ (Jinghe Materials, China), NCMOH424-a (Tianli Energy, China) and NCMOH424-b (Shijie New Energy, China)—were used to prepare NCM111 and NCM424. Stoichiometric of precursor and Li_2CO_3 were mixed in a molar ratio of Li:NCMOH = 1.05:1. Solid-state reactions were performed in a box furnace at a heating rate of 5 °C min^{-1}. A precalcination procedure was performed at 480 °C for 6 h. The synthesis temperature was then set from 900 to 1000 °C with a reaction time varied from 8 to 12 h. The furnace was purged with continuous airflow during the entire heating process and was then allowed to cool to room temperature naturally. The as-prepared samples were labeled according to their composition, synthesis temperature and time, e.g., NCM111-α-950-12h refers to the sample $Li(Ni_{1/3}Co_{1/3}Mn_{1/3})O_2$ synthesized at 950 °C for 12 h from the precursor NCMOH111-α.

Powder X-ray diffraction (XRD) measurements were performed using an XRD-6100 diffractometer (SHIMADZU, Japan) equipped with a Cu Kα radiation source; the diffractometer was operated at a step of 0.02° over a 2θ range from 10° to 80° to identify the structures and crystalline phases of the precursors and as-prepared compounds. The morphology of the precursors and as-prepared compounds were characterized using a scanning electron microscope (SEM, InTouchScope JSM-6010LA, JEOL, Japan) equipped with a tungsten filament operated at 20 keV.

The electrochemical performance was measured using CR2032 coin cells. The positive electrode was fabricated by mixing the active material with acetylene black (Timcal, Willebroek, Belgium) and polyvinyl difluoride (PVDF, Arkema Inc. Pennsylvania, USA) in *N*-methyl-2-pyrrolidone (NMP, MYJ Energy Tech., Puyang, China) at a weight ratio of 80:10:10. The blended slurries were evenly coated onto aluminum foil using a coating instrument and were subsequently completely dried. The electrode sheet was then punched into small discs with a diameter of 1.5 cm. The coin cells were assembled in an argon-filled glove box; Li metal was used as the anode, and porous polypropylene film was used as the separator. The electrolyte was 1 M $LiPF_6$ in ethylene carbonate (EC)/dimethyl carbonate (DMC) (1:1 by volume, Guotai-Huarong New Chemical Materials, Suzhou, China).

The cells were galvanostatically charged and discharged using a Dynamic Li-ion/Polymer Li-ion Battery Automatic Testing System (Chenwei Electronic Technology, China) at a current density of 0.1–3C in a voltage window of 3.0–4.3 V at room temperature.

3. Results and discussion

3.1. Characterization of the NCMOH precursors

The morphology, PPS, crystal structure and composition of the NCMOH precursors are of importance to the physical properties and electrochemical performance of the final NCM compounds, which were evaluated first. As shown in Fig. 1, all of the precursors had spheroidal secondary particles which are agglomerates of primary particle flakes. The tap densities of NCMOH111-α, NCMOH111-β, NCMOH111-γ, NCMOH424-a and NCMOH424-b were 2.26, 2.15, 2.27, 2.18 and 2.19 g cm^{-3}, respectively.

The crystal structure, lattice parameters and PPS of the precursors were evaluated by XRD (Fig. 2). Despite the presence of a $Co(OH)_2$ impurity phase (marked by asterisks), all precursors exhibited the same layered structure with space group *P-3m1*. Based on our previous results related to the synthesis of the NCM523 samples [11], this impurity has no obvious influence on the purity and properties of NCM compounds synthesized within the temperature range of 900–1000 °C.

The lattice parameters estimated by Le Bail fitting differ slightly from sample to sample, as listed in Table 1. The difference in the lattice parameters of the precursors has no obvious influence on the crystal structure of the final NCM products, as will be shown later in Section 3.2. The primary particles of the precursors were nanosized flakes, and the mean PPS estimated according to the Scherrer equation were 48.9, 57.8, 80.6, 91.6 and 79.8 nm for NCMOH111-α, NCMOH111-β, NCMOH111-γ, NCMOH424-a and NCMOH424-b, respectively. The original PPS of the precursors affected the PPS of the NCM products, which will be discussed in Section 3.2.

3.2. Effect of the precursors on the properties of NCM

To study the influence of the precursor on the properties of NCM, NCM samples were prepared using different NCMOH111 and NCMOH424 precursors with Li_2CO_3 at 950 °C for 12 and 9 h, respectively. The morphologies of the samples are shown in Fig. 3. The spheroidal morphologies of the precursors were retained after sintering. However, the shape and size of the primary particles changed from nanosheets in the precursors to larger polyhedrons that form the rough and textured secondary particle surface of NCM.

Detailed XRD analysis (Fig. 4) shows that all of the diffraction peaks can be fitted well with an α-$NaFeO_2$-type layered *R-3m* structure, which is same to the structure of NCM523 [11]; these results indicate that the compounds are single-phase and that the $Co(OH)_2$ impurity in the precursors does not affect the purity of the final as-prepared NCM compounds under the experimental synthesis conditions. The lattice parameters of the NCM samples are similar (Table 2). Considering the relatively big differences in lattice parameters between the precursors (Table 1), we can see no obvious relationship between the lattice parameters of the NCM and that of its precursor.

The PPS of the samples were estimated according to the Scherrer equation (Table 2). The precursors with smaller PPS values resulted in final NCM products with larger PPS values under the

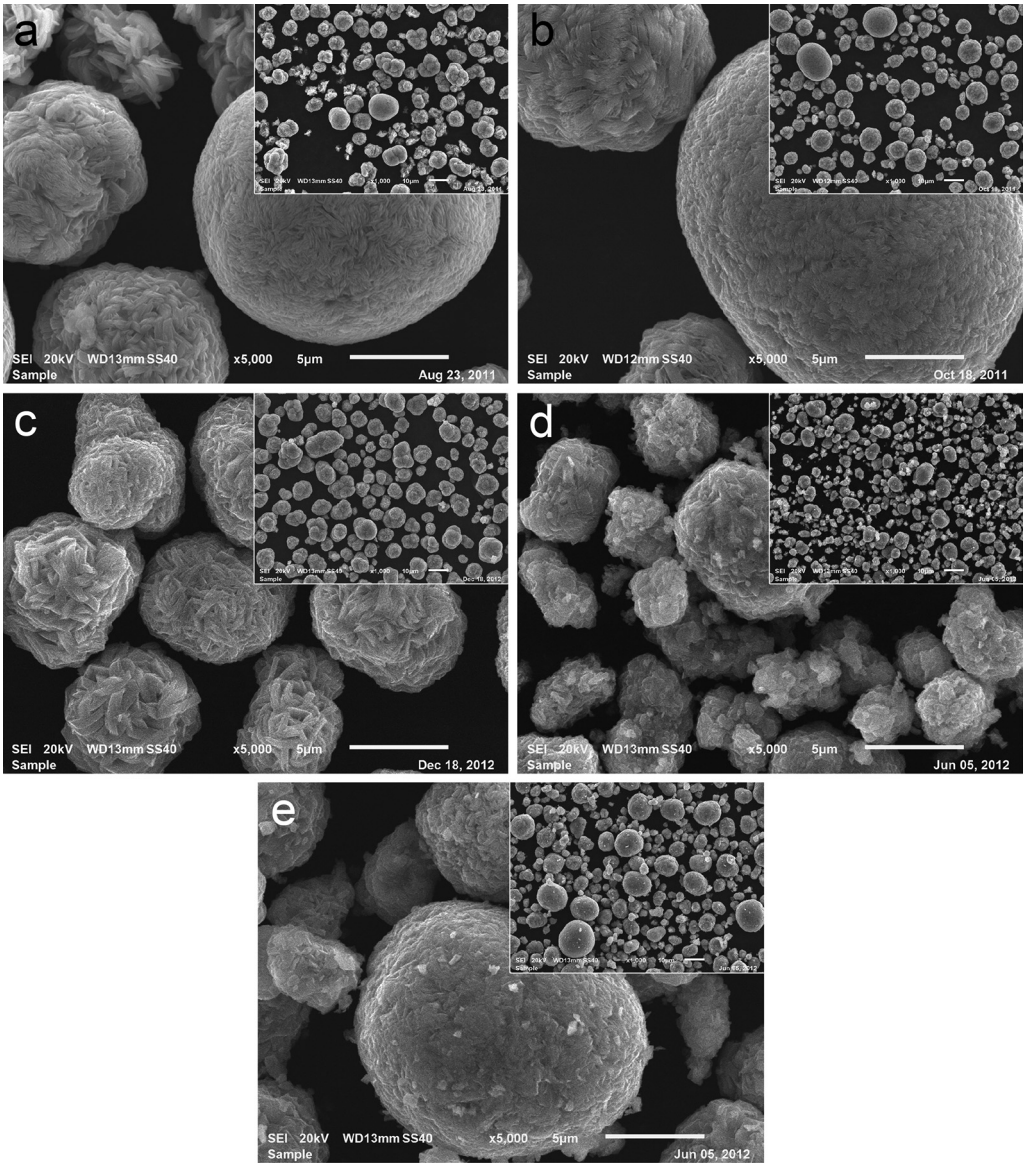

Fig. 1. SEM morphologies of the precursors NCMOH111-α (a), NCMOH111-β (b), NCMOH111-γ (c), NCMOH424-a (d) and NCMOH424-b (e).

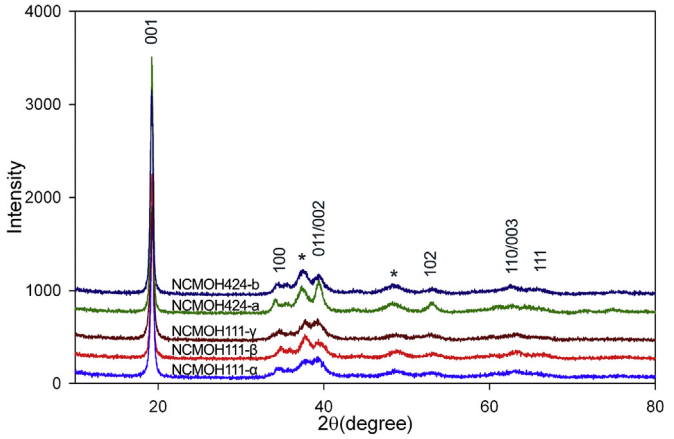

Fig. 2. XRD results of the precursors NCMOH111-α, NCMOH111-β, NCMOH111-γ, NCMOH424-a and NCMOH424-b, respectively. The asterisks marked the peaks belong to $Co(OH)_2$ impurity.

experimental synthesis conditions (Fig. S1). Specifically, $PPS_{NCM111\text{-}\alpha\text{-}950\text{-}12h} > PPS_{NCM111\text{-}\beta\text{-}950\text{-}12h} > PPS_{NCM111\text{-}\gamma\text{-}950\text{-}12h}$, whereas $PPS_{NCMOH111\text{-}\alpha} < PPS_{NCMOH111\text{-}\beta} < PPS_{NCMOH111\text{-}\gamma}$; and $PPS_{NCM424\text{-}a\text{-}950\text{-}9h} > PPS_{NCM424\text{-}b\text{-}950\text{-}9h}$, whereas $PPS_{NCMOH424\text{-}a} < PPS_{NCMOH424\text{-}b}$. A similar result was observed in a previous study of NCM523 [11]. The PPS of the final NCM compounds is also related to the morphology of the secondary particle size (SPS) of the precursor. It is evident from the results in Fig. 3b that the PPS of the smaller secondary particles on the right are larger than that of the larger secondary particles in the middle.

Table 1
Lattice parameters and mean PPS estimated from XRD by Le Bail fitting with tap densities of the precursors.

NCMOH	*a* (Å)	*c* (Å)	Mean PPS (nm)	Tap density (g cm^{-3})
NCMOH111-α	2.98348	4.61117	48.9	2.26
NCMOH111-β	2.98472	4.60375	57.8	2.15
NCMOH111-γ	2.96509	4.60228	80.6	2.27
NCMOH424-a	3.23124	4.48437	79.9	2.18
NCMOH424-b	3.23687	4.52913	86.1	2.19

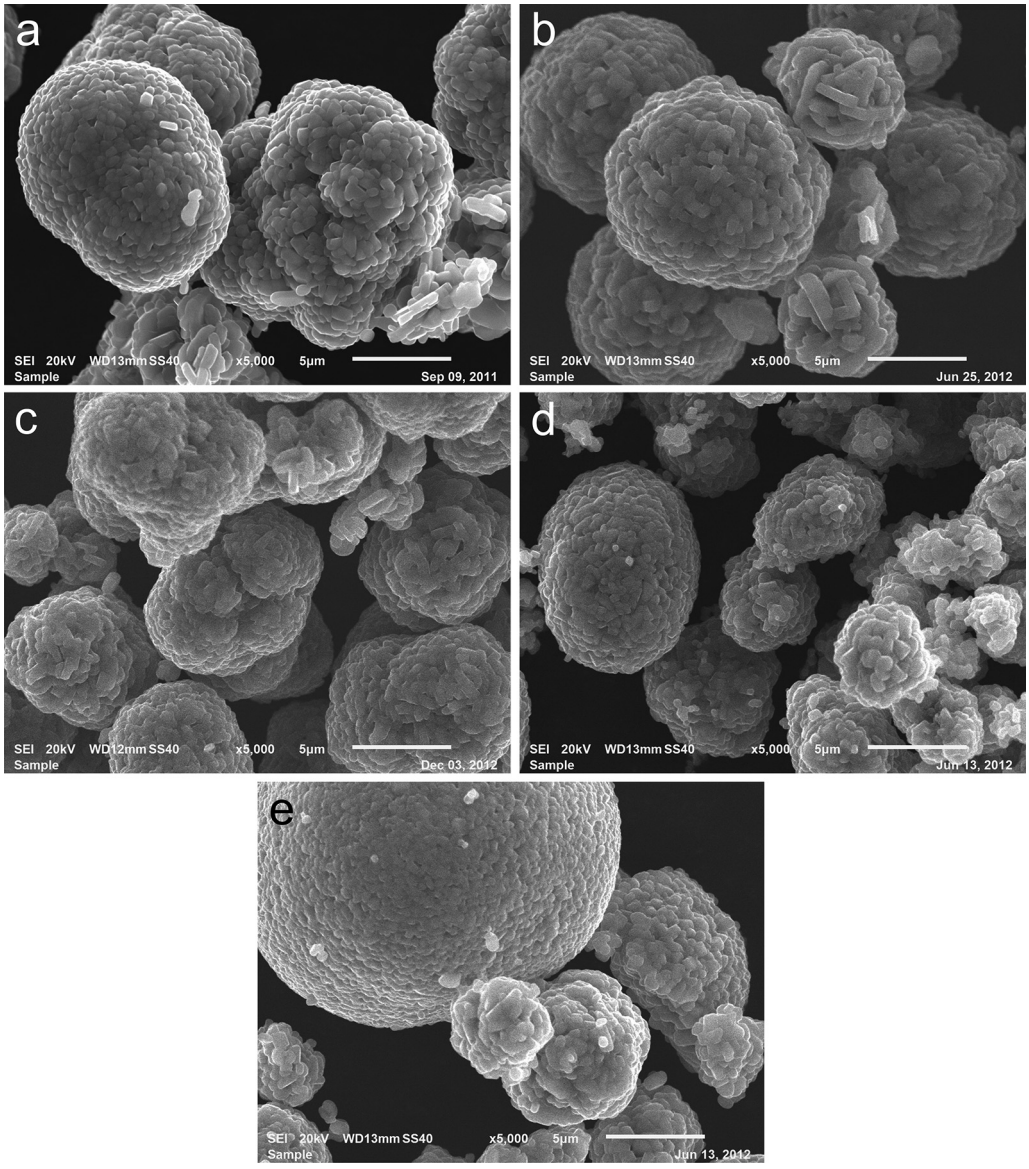

Fig. 3. SEM morphologies of the NCM111-α-950-12h (a), NCM111-β-950-12h (b), NCM111-γ-950-12h (c), NCM424-a-950-9h (d) and NCM424-b-950-9h (e).

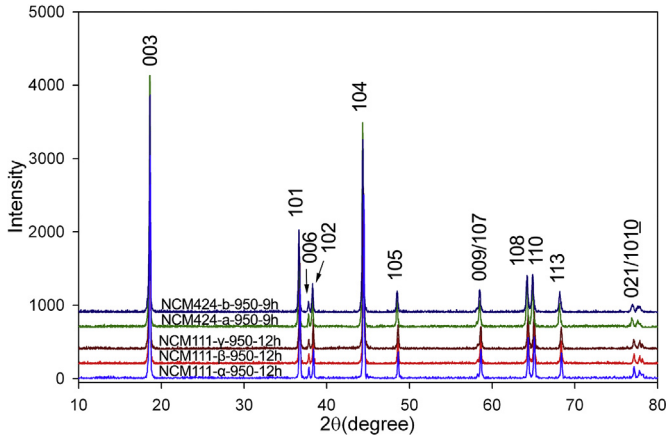

Fig. 4. XRD results of the NCM111-α-950-12h, NCM111-β-950-12h, NCM111-γ-950-12h, NCM424-a-950-9h and NCM424-b-950-9h.

NCM materials with higher crystallinity, better-defined hexagonal layered structures, less Ni^{2+}/Li^{+} antisite disordering and higher structural perfection exhibit better electrochemical performance [12–16], which is related to a larger c/a ratio and smaller I_{104}/I_{003} (where I_{hkl} is the integral intensity of the XRD peak (hkl) hereafter) ratios. These values were estimated from the XRD patterns, as listed in Table 2. NCM111-α-950-12h exhibited the highest

Table 2
Lattice parameters, mean PPS and intensity ratios of indicating peaks estimated from XRD by Le Bail fitting, and tap densities of the NCM compounds synthesized at 950 °C.

NCM	a (Å)	c (Å)	c/a	I_{104}/I_{003} (%)	Mean PPS (nm)	Tap density (g cm^{-3})
NCM111-α-950-12h	2.8625	14.2421	4.9754	86.30	463.1	2.30
NCM111-β-950-12h	2.8627	14.2355	4.9728	88.28	413.1	2.43
NCM111-γ-950-12h	2.8624	14.2394	4.9746	88.67	365.3	2.46
NCM424-a-950-9h	2.8712	14.2642	4.9680	88.97	376.3	2.27
NCM424-b-950-9h	2.8703	14.2622	4.9689	91.94	356.8	2.30

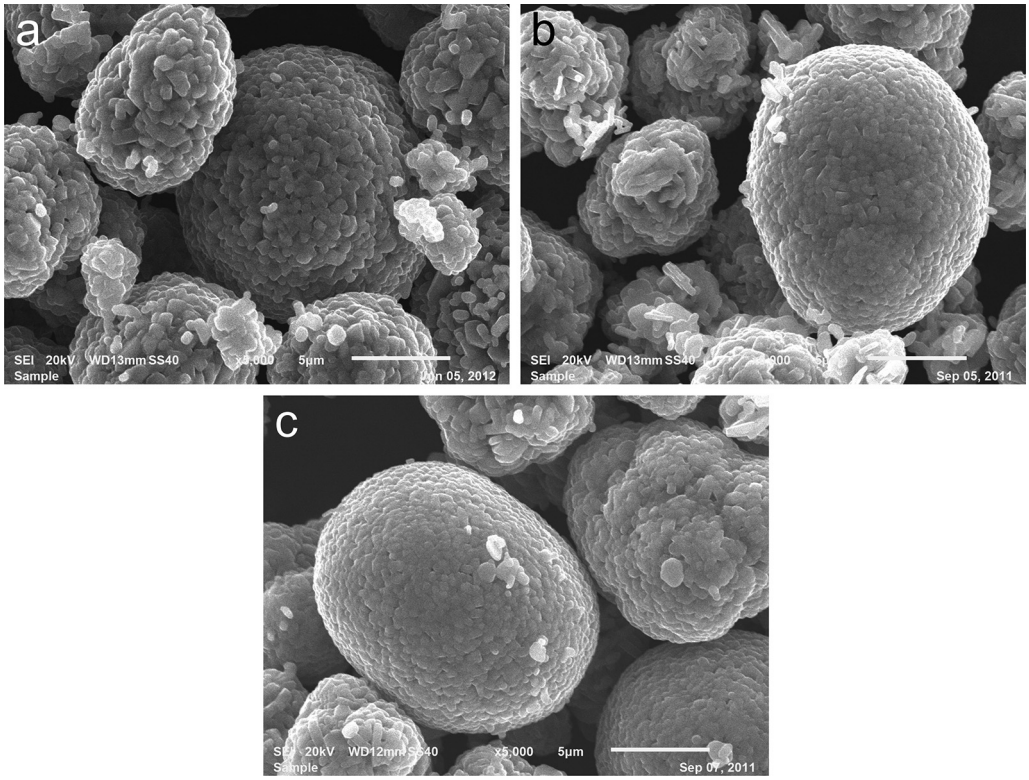

Fig. 5. SEM morphologies of the NCM111-α-920-8h (a), NCM111-α-920-10h (b), NCM111-α-920-12h (c).

c/*a* ratio of 4.9754, the lowest I_{104}/I_{003} ratio of 86.30%. Thus, we would expect NCM111-α-950-12h to exhibit the highest crystallinity, the best defined layered structure, the lowest degree of Ni^{2+}/Li^{+} antisite disordering and the greatest structural perfection among the NCM111 samples. Therefore, it should have the best electrochemical performance. Similarly, NCM424-a-950-9h has a much lower degree of Ni^{2+}/Li^{+} disordering and should exhibit a better performance than NCM424-b-950-9h. Thus, the precursors NCMOH111-α and NCMOH424-a were selected as the representative precursors for the subsequent investigation.

3.3. Effect of the reaction time on the properties of NCM

Fig. 5 shows the SEM images of the NCM111 synthesized with the precursor NCMOH111-α at 920 °C for 8, 10 and 12 h, respectively. The images show that the samples are similar with respect to their spheroidal morphology and polyhedral primary particle shapes. No obvious difference among the samples could be identified by SEM. However, the tap density of the NCM111 sample slightly decreased from 2.45 to 2.41 g cm^{-3} as the reaction time was increased from 8 to 12 h (Table 3, Fig. S2a). The laser particle sizing shows that the SPS of the samples were quite close to that of the NCMOH111-α precursor (D_{10} = 5.75 μm, D_{50} = 9.10 μm and D_{90} = 14.72 μm) and that the sample with a longer reaction time had a slightly larger SPS and a broader SPS distribution (Table 3, Fig. S2b). This difference implies that longer reaction time results in a lower tap density, a larger SPS and a broader SPS distribution of NCM111 under the current experimental conditions.

The XRD patterns of the samples are shown in Fig. 6, and the related information deduced from the XRD patterns is listed in Table 3. All of the samples are single phase with an α-$NaFeO_2$-type layered *R*-3*m* structure. The longer reaction time resulted in a larger PPS (Fig. S2a) and a larger *c*/*a* ratio in the NCM samples (Fig. S2c). These differences suggest that longer-reacted samples have better-defined layered character and crystallinity. The slightly larger SPS and lower tap density should be due to the slightly larger PPS that makes the secondary particles of the samples rougher; thus, more space exists among these secondary particles after tapping. The influence of the reaction time on the I_{104}/I_{003} ratio is not obvious (Fig. S2c), which implies that the reaction time has no direct effect on the level of Ni^{2+}/Li^{+} disordering and the structural perfection of NCM111 under the current experimental conditions.

3.4. Effect of the synthesis temperature on the properties of NCM

The synthesis temperature is one of the most important synthesis conditions; thus, its influence on the physical and electrochemical properties of NCM was studied intensively over the

Table 3
Lattice parameters, mean PPS and intensity ratios of indicating peaks estimated from XRD by Le Bail fitting, tap densities and SPS distributions of the NCM111-α synthesized at 920 °C for different reaction time.

NCM	*a* (Å)	*c* (Å)	*c*/*a*	I_{104}/I_{003} (%)	Mean PPS (nm)	T.D. (g cm^{-3})	SPS distribution (μm)		
							D_{10}	D_{50}	D_{90}
NCM111-α-920-8h	2.8623	14.2352	4.9733	88.92	391.5	2.45	5.81	9.26	14.65
NCM111-α-920-10h	2.8629	14.2386	4.9735	88.74	393.8	2.44	5.83	9.28	14.68
NCM111-α-920-12h	2.8631	14.2396	4.9735	88.89	397.5	2.41	5.85	9.31	14.72

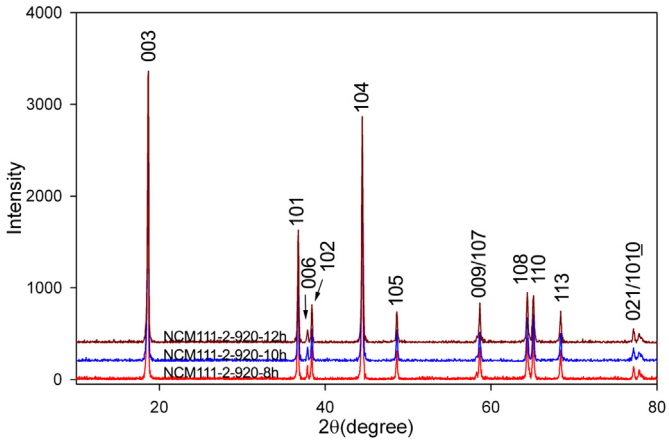

Fig. 6. XRD results of the NCM111-α-920-8h, NCM111-α-920-10h, NCM111-α-920-12h.

temperature range from 900 to 1000 °C. SEM micrographs of representative samples synthesized with the NCMOH111-α and NCMOH424-a precursors at different temperatures for 12 and 9 h are shown in Figs. 7 and 8, respectively. Similar to that of NCM523 [11], the PPS of NCM111 and NCM424 increased with increasing temperature (Fig. S3a and Fig. S4a). Quantitative results of the PPS estimated from the XRD results using the Scherrer equation (Figs. 9 and 10) are listed in Tables 4 and 5, respectively. This suggests that the PPS can be controlled through an adjustment of the synthesis temperature.

Laser particle size analysis shows that the SPS of the NCM111-α increases and that its distribution broadens with increasing synthesis temperature (Table 4, Fig. S3b). The tap density was also affected by the temperature, and the sample synthesized at a higher temperature exhibited a lower tap density (Fig. S3a). The large SPS and low tap densities of the samples synthesized at high temperatures is likely attributable to the agglomeration of small secondary particles of precursors during sintering. In addition, higher synthesis temperatures increase the probability of agglomeration. A larger PPS may also contribute to the low tap density.

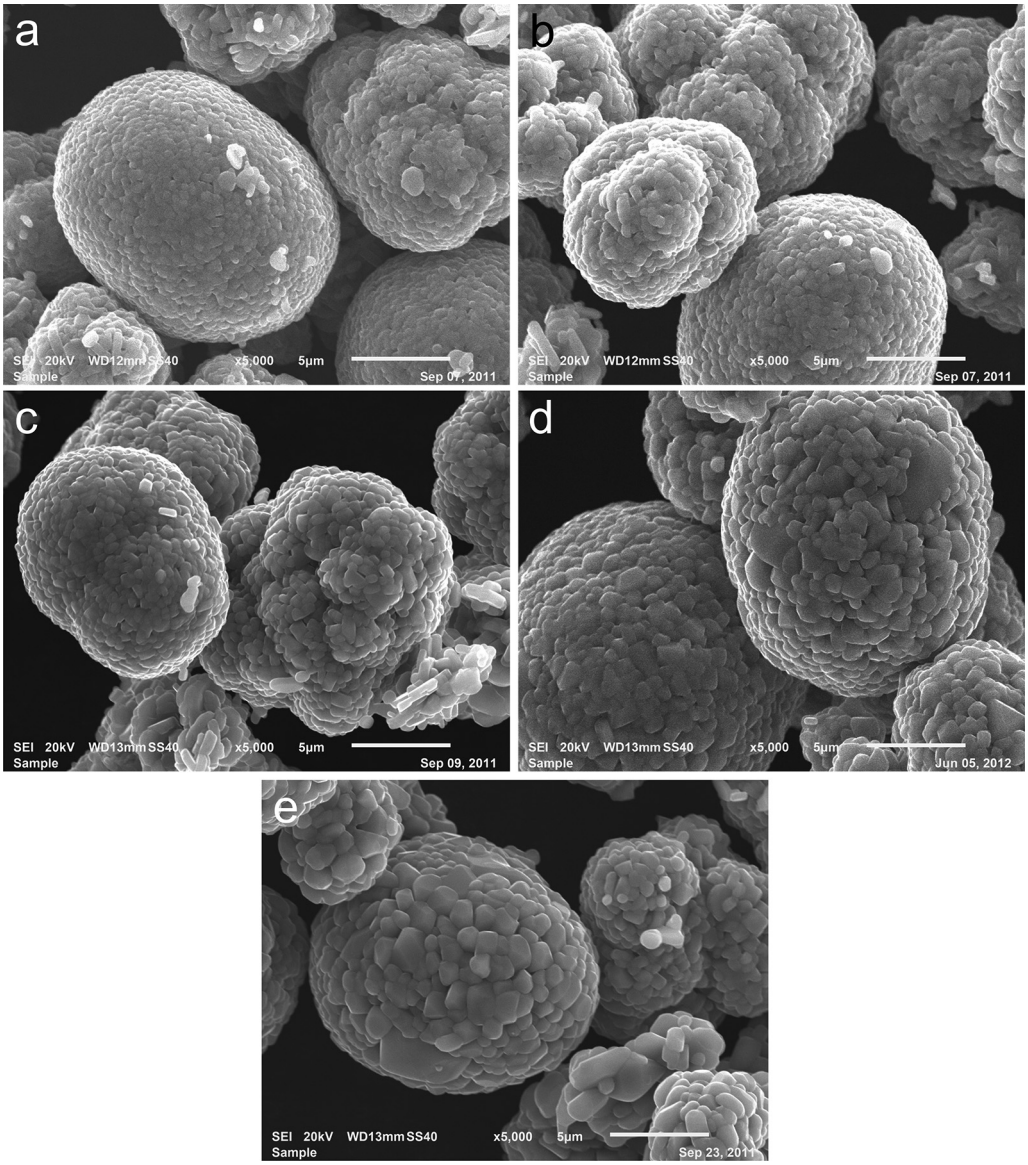

Fig. 7. SEM morphologies of the samples (a) NCM111-α-920-12h, (b) NCM111-α-940-12h, (c) NCM111-α-950-12h, (d) NCM111-α-970-12h and (e) NCM111-α-980-12h, respectively.

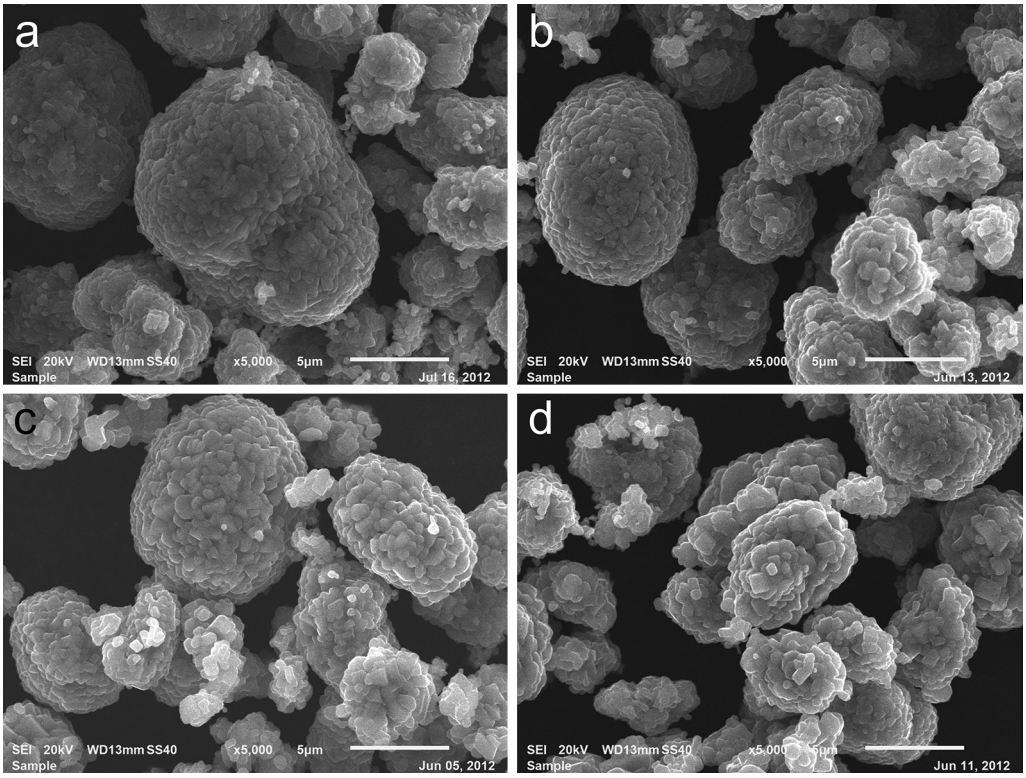

Fig. 8. SEM morphologies of the samples (a) NCM424-a-900-9h, (b) NCM424-a-950-9h, (c) NCM424-a-975-9h and (d) NCM424-a-1000-9h, respectively.

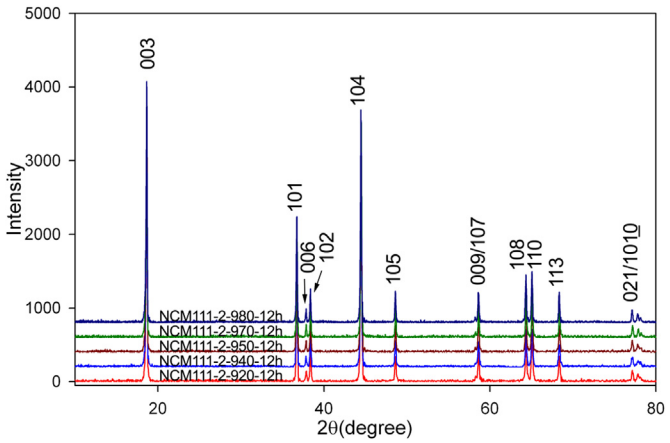

Fig. 9. XRD results of the NCM111-α-920-12h, NCM111-α-940-12h, NCM111-α-950-12h, NCM111-α-970-12h and NCM111-α-980-12h.

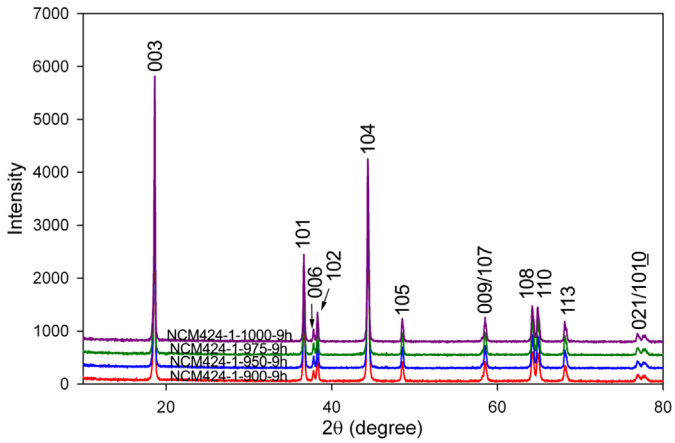

Fig. 10. XRD results of the NCM424-a-900-9h, NCM424-a-950-9h, NCM424-a-975-9h and NCM424-a-1000-9h.

The XRD analysis shows that all of the samples were single-phase with an α-$NaFeO_2$-type layered *R-3m* structure within the synthesis temperature range. The XRD peaks for both NCM111-α and NCM424-a become sharper and narrower when the synthesis temperature increases. This implies better crystallinity and larger PPS values. Moreover, the level of peak splitting for (006)/(102) and (108)/(110) also become more evident with increasing synthesis temperature, which suggests a better defined layered structure

Table 4
Lattice parameters, relative peak intensities, PPS, tap densities and SPS distribution of NCM111-α synthesized with precursor NCMOH111-α at different temperatures for 12 h.

NCM	*a* (Å)	*c* (Å)	*c*/*a*	I_{104}/I_{003} (%)	PPS (nm)	T.D. (g cm^{-3})	SPS distribution (μm)		
							D_{10}	D_{50}	D_{90}
NCM111-α-920-12h	2.8631	14.2396	4.9735	88.89	397.5	2.41	5.85	9.31	14.72
NCM111-α-940-12h	2.8629	14.2426	4.9750	86.68	432.1	2.36	5.92	9.95	16.65
NCM111-α-950-12h	2.8625	14.2421	4.9754	86.30	463.1	2.30	6.00	10.13	17.03
NCM111-α-970-12h	2.8611	14.2319	4.9742	86.34	485.9	2.27	6.54	11.74	20.83
NCM111-α-980-12h	2.8633	14.2415	4.9739	86.42	495.2	2.25	6.82	12.35	22.07

Table 5
Lattice parameters, relative peak intensities and PPS of NCM424-a synthesized with precursor NCMOH424-a at different temperatures for 9 h.

NCM	a (Å)	c (Å)	c/a	I_{104}/I_{003} (%)	PPS (nm)
NCM424-a-900-9h	2.8712	14.2646	4.9682	91.80	319.3
NCM424-a-950-9h	2.8712	14.2642	4.9680	88.97	376.3
NCM424-a-975-9h	2.8716	14.2636	4.9671	88.72	408.9
NCM424-a-1000-9h	2.8717	14.2627	4.9666	90.75	411.3

[17,18]. Details of the crystal structure and relative peak intensities were estimated by XRD Le Bail fitting; the results are listed in Tables 4 and 5 for NCM111-α and NCM424-a, respectively. With increasing synthesis temperature, the c/a ratio of NCM111-α increases and reaches a maximum at 950 °C after which it decreases. The I_{104}/I_{003} value decreases with increasing synthesis temperature, reaches its minimum at 950 °C and then increases after that (Fig. S3c). From comprehensive considerations, the NCM111-α-950-12h sample synthesized at 950 °C should exhibit the highest crystallinity, greatest structural perfection and a hexagonal layered structure with a low level of Ni^{2+}/Li^{+} disordering; this sample should therefore exhibit the best electrochemical performance [19,20] among the samples synthesized within the investigated temperature range.

Similarly, XRD analysis shows that the NCM424-a-950-9h synthesized at 950 °C exhibits the best combination of high crystallinity, a well-defined layered structure and a low level of cation disordering (Fig. S4b). This sample should exhibit the best electrochemical performance among the NCM424 samples [19,20].

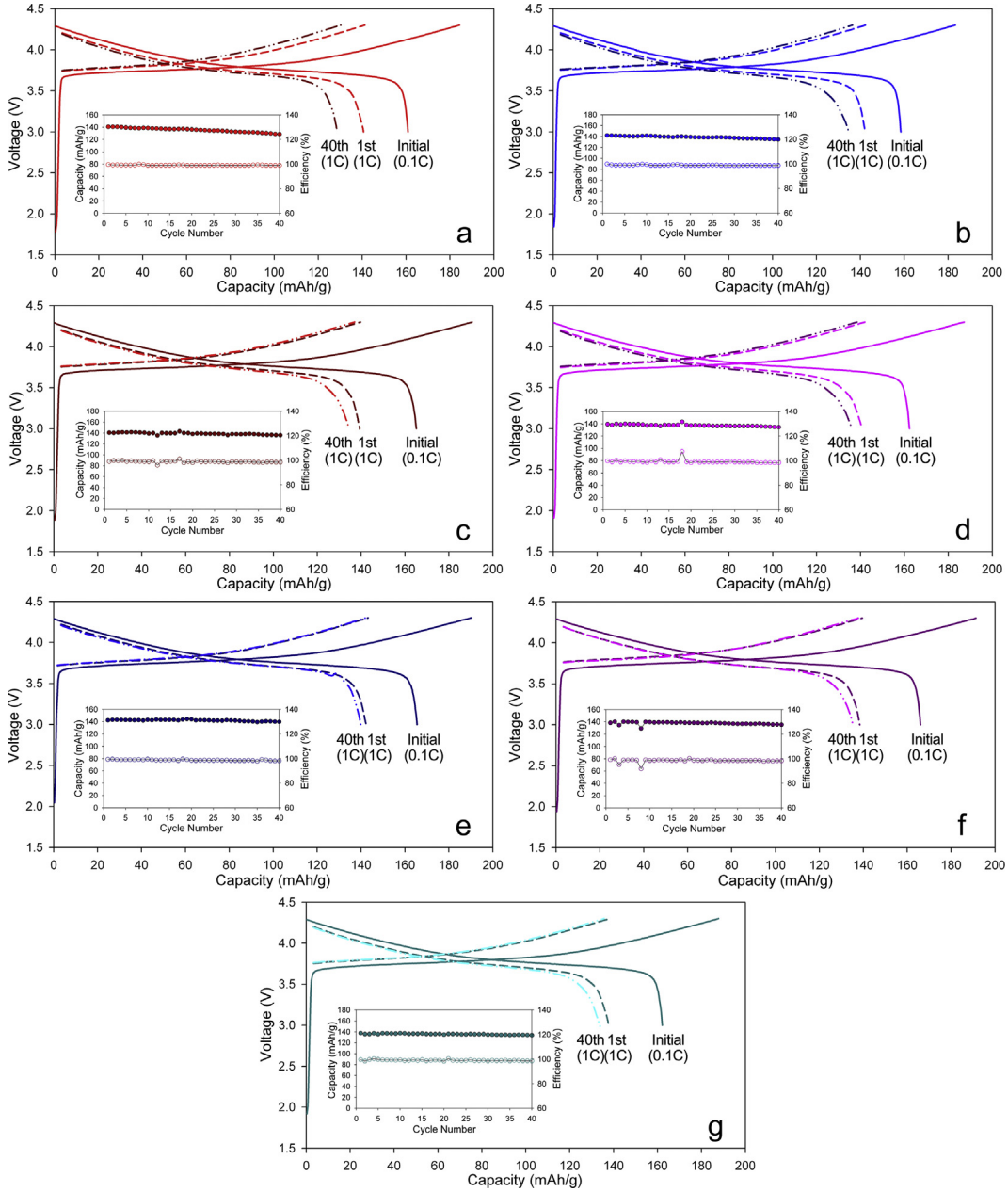

Fig. 11. Charge/discharge voltage profiles for the initial (0.1C), 1st (1C) and 40th (1C) cycles with 1C cyclability (filled circles) and efficiency (open circles) of (a) NCM111-α-920-8h, (b) NCM111-α-920-10h, (c) NCM111-α-920-12h, (d) NCM111-α-940-12h, (e) NCM111-α-950-12h, (f) NCM111-α-970-12h and (g) NCM111-α-980-12, respectively.

Table 6
Electrochemical performance of the NCM111-α samples synthesized with precursor NCMOH111-α in different conditions.

Sample	Initial cycle			Rate capability			1C cyclability		
	Charge (mAh g^{-1})	Discharge (mAh g^{-1})	Coulombic efficiency (%)	1C discharge (mAh g^{-1})	3C discharge (mAh g^{-1})	3C rate (%)	1st discharge (mAh g^{-1})	40th discharge (mAh g^{-1})	Retention rate (%)
NCM111-α-920-8h	184.3	160.9	87.3	142.3	131.3	92.27	140.6	128.7	91.54
NCM111-α-920-10h	183.2	158.4	86.5	143.0	133.0	93.01	142.2	134.6	94.66
NCM111-α-920-12h	187.2	162.1	86.7	142.3	129.2	90.79	139.4	135.5	96.48
NCM111-α-940-12h	190.5	165.1	86.6	144.5	131.5	91.00	140.6	136.1	96.80
NCM111-α-950-12h	190.2	165.5	87.0	146.3	133.5	91.25	142.3	139.8	98.25
NCM111-α-970-12h	191.3	166.0	86.8	143.5	131.0	91.29	138.4	135.3	97.76
NCM111-α-980-12h	187.8	162.2	86.4	141.2	128.5	91.01	137.7	133.8	97.17

It was found in our previous work that the optimum synthesis temperature for NCM523 is 880 °C [11], which is lower than the optimum synthesis temperature of 950 °C determined for NCM111 and NCM424. It is proposed that, when the Ni content of NCM is decreased, an elevated optimum synthesis temperature is required to prepare a high-performance compound with better physical properties.

In general, the I_{104}/I_{003} ratio for NCM424 (approximately 90%) is larger than that of NCM111 (normally less than 89%), which indicates a higher level of Ni^{2+}/Li^{+} disordering in NCM424. Furthermore, NCM523 has a larger I_{104}/I_{003} ratio (typically greater than 90%) than the other two species [11]. This difference suggests that the higher Ni^{2+} content results in a higher level of Ni^{2+}/Li^{+} disordering (larger I_{104}/I_{003} ratio). This increased disordering is because more Ni^{2+} in the transition metal layer provides more opportunities for Ni^{2+}/Li^{+} disordering to occur.

3.5. Electrochemical properties study

The electrochemical performance of the NCM samples synthesized under different conditions was compared to explore the influence of the synthesis conditions, as shown in Fig. 11 and Table 6. Fig. 11 shows the voltage profiles of the initial (0.1C), 1st (1C), and 40th (1C) charge/discharge cycles and the corresponding cycling performance and coulombic efficiency (1C, insets) of Li/NCM111-α cells cycled between 3.0 and 4.3 V. The potential plateau at 3.75 V corresponds to the Ni^{2+}/Ni^{4+} redox couple [12]. Detailed results (Table 6) show that, during the initial charge, a capacity less than 187.2 mAh g^{-1} was drawn from the samples synthesized at 920 °C and a capacity no greater than 162.1 mAh g^{-1} was recovered during the initial discharges, which corresponds to 86.5–87.3% of the initial charge capacity. The samples synthesized over shorter times tend to have higher rate capabilities, which is due to their smaller PPS (Fig. S5a). Although the samples synthesized over shorter times have a higher first-cycle 1C discharge capacity, repeated cycling resulted in rapid decreases in discharge capacity. The capacity retention rate at 1C after 40 cycles increased from 91.54% to 96.48% as the reaction time was increased from 8 to 12 h (Fig. S5a). The better cyclability of NCM111-α-920-12h is likely attributable to its large PPS, high crystallinity and its well-defined layered structure, as shown in Table 3. After 40 cycles, the discharge capacity of NCM111-α-920-12h exceeded that of the other two samples synthesized at 920 °C.

For the samples sintered at different temperatures for 12 h, the initial charge/discharge capacity at 0.1C and the rate capability at 3C increased gradually to 191.3/166.0 mAh g^{-1} and 91.29%, respectively, when the synthesis temperature was increased to 970 °C and then decreased after that (Table 6). The initial coulombic efficiency, the discharge capacities at 1C and 3C and the retention rate at 1C after 40 cycles also increased with increasing synthesis temperature. However, these properties reached their maximum values for samples synthesized at 950 °C and then decreased when the synthesis temperature was increased further. Thus, NCM111-α-950-12h exhibited the best overall electrochemical performance.

The electrochemical performance of the samples is predictable from the corresponding physical properties, especially the PPS and crystal structure, which are determined by the nature of the precursors and the synthesis conditions. First, on the basis of the XRD analyses (see Table 4), NCM111-α-950-12h and NCM111-α-970-12h have the smallest I_{104}/I_{003} (Fig. S3c), which implies that these two samples have a lower level of Ni^{2+}/Li^{+} disordering and a higher structural perfection. Therefore, these two samples should exhibit higher rate capabilities and better cyclabilities than the other samples (Fig. S5c); second, NCM111-α-950-12h had the highest c/a ratio (Fig. S3c), which suggests that it should exhibit the highest crystallinity, the most well-defined layer structure and the best cycling stability (Fig. S5b). In summary, NCM111-α-950-12h has low Ni^{2+}/Li^{+} disordering, a well-defined layered, hexagonal structure and good crystallinity, which, together with its appropriate PPS, offers a high capacity, high coulombic efficiency, high rate capability and good cycling performance.

These results show that the electrochemical performance of NCM materials is directly related to their physical properties (Fig. S5), which are tunable through changes in the precursor and synthesis conditions, especially the synthesis temperature and the reaction time.

4. Conclusion

Single-phase $Li(Ni_{1/3}Co_{1/3}Mn_{1/3})O_2$ and $Li(Ni_{0.4}Co_{0.2}Mn_{0.4})O_2$ compounds with a layered structure and spheroidal morphology were synthesized using the corresponding commercially supplied precursors NCMOH111-α, NCMOH111-β, NCMOH111-γ, NCMOH424-a and NCMOH424-b. The physical properties and electrochemical performances of the samples depend highly on the choices of precursors, synthesis temperature and reaction time. We found that:

(1) Larger PPS and SPS of the precursors made a smaller PPS of NCM. NCM with smaller PPS has a higher rate capability but a worse cyclability;
(2) Extending the reaction time led to slightly larger PPS and SPS, a better crystallinity and layered structure of NCM, resulting in a slightly lower tap density and substantially improved cyclability of NCM;
(3) Higher synthesis temperatures resulted in larger PPS and SPS, broader SPS distributions and lower tap densities of NCM;
(4) NCM with better crystallinity, a well-defined layered structure and better cation ordering exhibited a higher specific capacity, better cycling performance and better rate capability;
(5) The level of Ni^{2+}/Li^{+} disordering was higher with higher Ni^{2+} content. And when the Ni content was decreased, an elevated synthesis temperature was required to prepare an

NCM compound with the appropriate physical properties and high electrochemical performance.

The optimized synthesis conditions for precursors NCMOH111-α and NCMOH424-a under the current experimental conditions were 950 °C for 12 h and 950 °C for 9 h, respectively. The NCM111-α-950-12h sample delivered a discharge capacity of 165.5 mAh g^{-1} during the initial cycle at 0.1C with a columbic efficiency of 87%, a 3C rate capability of 91.25% and a 1C capacity retention rate of 98.25% after 40 cycles.

Acknowledgments

This work were supported by the Cixi Scientific and Technological Plans and Achievement Transformation Project of Cixi City, China (No: 2011A10), 973 Program (2011CB933300), National Natural Science Foundation of China (51071110, 40972044, 51271134, J1210061), China MOE NCET Program (NCET-07-0640), MOE Doctoral Fund (20090141110059), 863 Program (2013AA050901), and the Fundamental Research Funds for the Central Universities. The authors gratefully acknowledge Dr. Hongjun Niu from the University of Liverpool for valuable suggestions.

Appendix A. Supplementary data

Supplementary data related to this article can be found at http://dx.doi.org/10.1016/j.jpowsour.2013.09.064.

References

[1] Y. Chen, G.X. Wang, K. Konstantinov, H.K. Liu, S.X. Dou, J. Power Sources 119–121 (2003) 184–188.
[2] T. Ohzuku, Y. Makimura, Chem. Lett. (2001) 642–643.
[3] Y. Koyama, I. Tanaka, H. Adachi, Y. Makimura, T. Ohzuku, J. Power Sources 119–121 (2003) 644–648.
[4] Y.K. Sun, S.T. Myung, B.C. Park, J. Prakash, I. Belharouak, K. Amine, Nat. Mater. 8 (2009) 320–324.
[5] S. Patoux, M.M. Doeff, Electrochem. Commun. 6 (2004) 767–772.
[6] I. Belharouak, Y.K. Sun, J. Liu, K. Amine, J. Power Sources 123 (2003) 247–252.
[7] X.Y. Zhang, W.J. Jiang, A. Mauger, Qilu, F. Gendron, C.M. Julien, J. Power Sources 195 (2010) 1292–1301.
[8] X.F. Luo, X.Y. Wang, L. Liao, S. Gamboa, P.J. Sebastian, J. Power Sources 158 (2006) 654–658.
[9] C. Deng, L. Liu, W. Zhou, K. Sun, D. Sun, Electrochim. Acta 53 (2008) 2441–2447.
[10] S. Zhang, Electrochim. Acta 52 (2007) 7337–7342.
[11] K. Wu, F. Wang, L. Gao, M.-R. Li, L. Xiao, L. Zhao, S. Hu, X. Wang, Z. Xu, Q. Wu, Electrochim. Acta 75 (2012) 393–398.
[12] J.R. Dahn, U. von Sacken, C.A. Michal, Solid State Ionics 44 (1990) 87–97.
[13] J.N. Reimers, E. Rossen, C.D. Jones, J.R. Dahn, Solid State Ionics 61 (1993) 335–344.
[14] R.V. Moshtev, P. Zlatilova, V. Manev, A. Sato, J. Power Sources 54 (1995) 329–333.
[15] M. Yoshio, Y. Todorov, K. Yamato, H. Noguchi, J.-I. Itoh, M. Okada, T. Mouri, J. Power Sources 74 (1998) 46–53.
[16] Z. Wang, H. Dong, L. Chen, Y. Mo, X. Huang, Solid State Ionics 175 (2004) 239–242.
[17] J.H. Kim, C.S. Yoon, Y.K. Sun, J. Electrochem. Soc. 150 (2003) A538–A542.
[18] J.-M. Kim, H.-T. Chung, Electrochim. Acta 49 (2004) 937–944.
[19] C.-y. Hu, J. Guo, X.-y. Wang, Chin. J. Nonferrous Met. 18 (2008) 1721–1726.
[20] H.-j. Guo, M. Zhang, X.-h. Li, X.-m. Zhang, Z.-x. Wang, W.-j. Peng, M. Hu, Trans. Nonferrous Met. Soc. China 15 (2005) 1185–1189.